Reprinted from ENVIRONMENTAL SCIENCE & TECHNOLOGY, Vol. 28, 1994

Role of Combustion and Sorbent Parameters in Prevention of Polychlorinated Dibenzo-*p*-dioxin and Polychlorinated Dibenzofuran Formation during Waste Combustion

Brian K. Gullett* and Paul M. Lemieux

Air and Energy Engineering Research Laboratory, U.S. Environmental Protection Agency, Research Triangle Park, North Carolina 27711

James E. Dunn

Department of Mathematical Sciences, University of Arkansas, Fayetteville, Arkansas 72701

This research uses experimental data and a statistical approach to determine the effect of combustion- and sorbent-injection-related parameters on the mechanism of polychlorinated dibenzo-*p*-dioxin and polychlorinated dibenzofuran (PCDD and PCDF, respectively) formation and prevention in waste combustors. The operation of a pilot-scale combustor was varied to effect different regimes of oxygen (O_2), hydrogen chloride (HCl), and chlorine (Cl_2) concentration; temperature; residence time; quench rate; and sorbent injection. The fly ash loading of a municipal waste combustor was simulated by postcombustion injection of fly ash collected from a full-scale facility. Downstream sampling and analysis indicated significant PCDD and PCDF formation, beyond concentrations on the preinjected fly ash, at rates conducive to explaining formation in full-scale facilities at particle/gas residence times <5 s. Stepwise regression analyses determined the predictive parameters for four models of PCDD, PCDF, the total of PCDD and PCDF yield, and the partitioning between PCDD and total yield. Substantial prevention of PCDD and PCDF formation can be brought about with upstream sorbent injection for HCl and Cl_2 reduction, control of excess air, and increased quench rate.

Introduction

Overview. In recent years the focus on polychlorinated dibenzo-*p*-dioxin (PCDD) and polychlorinated dibenzofuran (PCDF) formation in municipal waste combustion (MWC) facilities has shifted from incomplete destruction of the feed to a low temperature, downstream mechanism of formation on the surface of fly ash. This shift was brought about in large part by theoretical analyses (*1*, *2*) of PCDD and PCDF formation models at combustion temperatures and is supported now by numerous results from field sampling programs (*3*–*5*) in which PCDD and PCDF concentrations were greater in downstream duct flue gas than in the immediate postfurnace gases. Laboratory research simulating postfurnace temperature and gas conditions of MWCs (for example, refs 6–14) has additionally implicated the role of fly ash in promoting downstream PCDD and PCDF formation.

Organics Source. A theory has been proposed (*15*) for *de novo* synthesis of PCDD and PCDF from chemically unrelated organic carbon sources and inorganic chlorine (Cl) compounds in the presence of a metal catalyst. Experimental evidence has shown that particle-bound carbon (C) on the fly ash reacts with oxygen (O_2), water (H_2O), and inorganic chlorides via a copper [Cu(II)] catalyzed reaction to form aromatic structures including chlorinated organics, PCDD, and PCDF (*16*). An alternative theory proposes that fly ash constituents are involved in heterogeneous catalytic reactions to form biaryl structures, including PCDD and PCDF, from chloroorganic precursors (*6*, *17*). Comparative testing of the two theories found that PCDD yields from pentachlorophenol precursors were 2–4 orders of magnitude greater than those from the *de novo* synthesis of combined particulate C, inorganic chlorides, and a Cu catalyst (*18*, *19*). Nonetheless, the difficulties in establishing independent control of the parameters of interest in the field coupled with difficulties in simulating combustion conditions in the laboratory suggest that both theories may be valid, each offering plausible mechanisms for formation of PCDD and PCDF in MWCs.

Chlorine Source. A source of Cl for the organic precursors may be provided through the metal (*M*) catalyzed Deacon reaction (*20*):

$$2HCl + 1/2O_2 \overset{M}{\rightleftharpoons} Cl_2 + H_2O \qquad (1)$$

This was implicated by Griffin (*21*) and demonstrated by others (*14*, *22*).

Equilibrium analyses (*23*) indicate favorable formation of Cl_2 over that of HCl as temperatures drop below ≈900 °C for an oxygen-rich (O), hydrogen-lean (H) system. Concentrations of Cl_2 of ≈50 ppmv may be typical for a MWC (*21*), although sampling data are scarce.

The ability of Cl_2 to readily chlorinate aromatics has been shown in the presence (*24*) and absence of fly ash (*25*) and likely occurs via a substitution reaction (*26*). Research (*7*, *9*) has shown that unchlorinated dibenzodioxin and 1,2,3,4-TCDD can be readily chlorinated by HCl at temperatures ranging up to 250 °C if they are adsorbed on fly ash. Similarly, HCl readily reacts with toluene in the presence of a fly ash catalyst to form chlorinated biphenyl, PCDD, and PCDF (*27*). Experiments with both HCl and Cl_2 sources without fly ash surfaces indicate that chlorination of phenol is over 4 orders of magnitude greater with Cl_2 than with HCl (*25*).

Effect of Oxygen. There is consensus in the literature among the laboratory-, pilot-, and field-scale researchers that formation of PCDD and PCDF is dependent upon O_2 concentration. Researchers (*11*) have found that increasing concentrations of O_2 from 0 to 10% resulted in the greater production of PCDD and PCDF (fly ash tests, 300 °C, 2 h). Others (*28*) demonstrated that an increased air to fuel ratio (0.8–1.2) led to higher levels of PCDD and PCDF during fluidized combustion of model waste materials. The effect of O_2 on the Deacon reaction is thought to produce Cl_2, leading to organochlorine formation and

then PCDD and PCDF (*14*). This dependency of Cl_2 formation from HCl through eq 1 has been shown on the bench-scale to be linearly dependent on O_2 concentration up to 3%, after which conversion remains constant to 10% (*29*). In experiments with C as the organic source (18), PCDD yields increased with O_2 supply, reflecting the dependency of the Deacon reaction and phenol formation (an intermediate in production of PCDD and PCDF) on O_2 concentration. Experiments with pentachlorophenol (PCP) as the organic source showed contradictory trends: direct formation of octachlorodioxin from the condensation of two PCP molecules was found to be independent of the presence of O_2 in one case (*18*), while fly ash experiments (300 °C) with PCP and tetrachlorobenzene showed that the presence of O_2 led to a greater yield of PCDD and PCDF and a product distribution shifted toward higher chlorinated species than tests with nitrogen (N_2) alone (*30*). Others (*8*) have found that the absence of O_2 promotes decomposition of PCDD and PCDF via a dechlorination/hydrogenation reaction (*14*).

Temperature. Isothermal, fixed bed, bench-scale experiments (*12*) with MWC fly ash plugs have shown that maximum PCDD and PCDF formation occurs around temperatures of 300 °C with an effective range of 250–400 °C (*11*). Experiments with nonfly ash PCDD and PCDF precursors (phenol, Cl_2, O_2, and CuO catalyst) have shown maximum formation temperatures around 400 °C (*31, 22*) while pentachlorophenol experiments suggest maximums around 250–300 °C (*19*).

Quench Rate. To our knowledge, only limited experiments on the effect of varying quench rate upon PCDD and PCDF yield have been reported. These small pilot-scale, fluidized-bed results (*32*) suggested that higher quench rates formed less PCDD and PCDF.

Residence Time. Scant information is available concerning residence time effects and, hence, the rate of PCDD and PCDF formation. This is due to reliance (primarily) upon fixed bed isothermal experiments of long duration (minutes to hours) that collect cumulative PCDD and PCDF yield data. Theoretical work (*33*) has shown that, despite diffusive transport limitations of gaseous precursors and evidence (with PCP) for incomplete precursor conversions (*17*), field PCDD and PCDF concentrations could be explained by the reaction between gaseous precursors and in-flight fly ash particles under reasonable temperature/time constraints. Laboratory rate data are only beginning to support this mechanism. Tests with a PCP precursor showed that the maximum rate of observed PCDD and PCDF formation based on sampling time, not gas/solid contact time, is 147 ng (g of fly ash)$^{-1}$ s^{-1} (*19*), sufficient to explain all but the higher field-sampled concentrations (*34*). If this maximum observed reaction rate measurement is a valid approximation of the rate-limiting step in PCDD and PCDF formation, then field concentrations do not have to be explained by a mechanism involving the reaction of surface-bound particles with eventual reentrainment and/or volatilization (*34*). This has significant implications for control devices and duct walls where deposited particle residence times significantly exceed those of in-flight particles.

Sorbent Work. Sorbents, most typically $Ca(OH)_2$, are often used for control of hydrochloric acid gases in MWCs. Recently, attention has focused on the ability of sorbents to remove PCDD and PCDF. Carlsson (*35*) reported a comparison of PCDD and PCDF emissions after various air pollution control processes including dry scrubbers with fabric filter (>98% removal), spray dryers with electrostatic precipitators (ESPs) (74–97% removal), ESPs with condensation scrubbers (62% removal), and ESPs with adiabatic scrubbers (89% removal). These PCDD and PCDF emission reductions are likely due to an adsorption mechanism on the sorbent surface followed by collection of the sorbent particles in a particulate control device. This is supported by scrubber results (*36*) that show typically ≈50% PCDD and PCDF removal prior to a fabric filter, increasing to >99.8% after the fabric filter.

The effect of dolomitic limestone ($CaCO_3$–$MgCO_3$) addition to a fluidized bed waste combustor led to PCDD and PCDF yield reductions in proportion to the decline in HCl concentration (*37*). Similar results can be inferred from data (*38*) in pilot plant work. These apparent effects are difficult to document conclusively due to the many uncontrollable variables involved in field trials. Indeed, other researchers (*39*) were unable to correlate the MWC emissions of PCDD and PCDF with HCl concentration. Laboratory and pilot-scale data are also lacking. While laboratory investigations of reaction kinetics (*40, 41*) and field results (*42–45*) indicate rapid and extensive reductions in HCl concentrations by sorbent addition, no effort has been made to link HCl reductions with PCDD and PCDF yield decreases at the laboratory or pilot scale. Although a role for HCl and metal chlorides in the PCDD and PCDF formation mechanism appears clear, it is less clear whether the formation of trace amounts of PCDD and PCDF is related to HCl concentration. It is possible that the formation of PCDD and PCDF in downstream regions of MWCs is essentially a zero-order process in HCl concentration and that some other mechanistic step is rate limiting.

Summary. Extensive characterization of the mechanism of PCDD and PCDF formation is made difficult by the inability to accurately simulate the combustion/fly ash environment and to control the experimental parameters that effect PCDD and PCDF formation. Several groups have done correlative analyses on pilot-scale data, attempting to determine the important parameters that effect downstream PCDD and PCDF formation (*32, 46–49*). Their work has determined some preliminary associations; in most cases, the conclusions were limited by the ability to control furnace parameters and make meaningful determinations. In the research reported here, controlled variation of mechanistic parameters at the pilot-scale allows verification of bench-scale findings, while realistically simulating the combustion gas composition, the gas/particle dynamics, the condensed compounds expected on the fly ash, the *in situ* catalytic action, and the relevant temperature regimes of a full scale MWC. A statistical analysis of the results from varying these parameters enables mechanistic determinations that will recommend ways of preventing or reducing the formation of PCDD and PCDF compounds.

Experimental Section

Furnace. Tests were run on a pilot-scale 14.7-kW (63 000 Btu/h), refractory-lined, down-fired cylindrical furnace fired with natural gas (Figure 1). The furnace, termed the "Innovative Furnace Reactor" (IFR), has an inner diameter of 15.2 cm and an overall vertical length of about 4 m. View and injection/probe ports traverse the

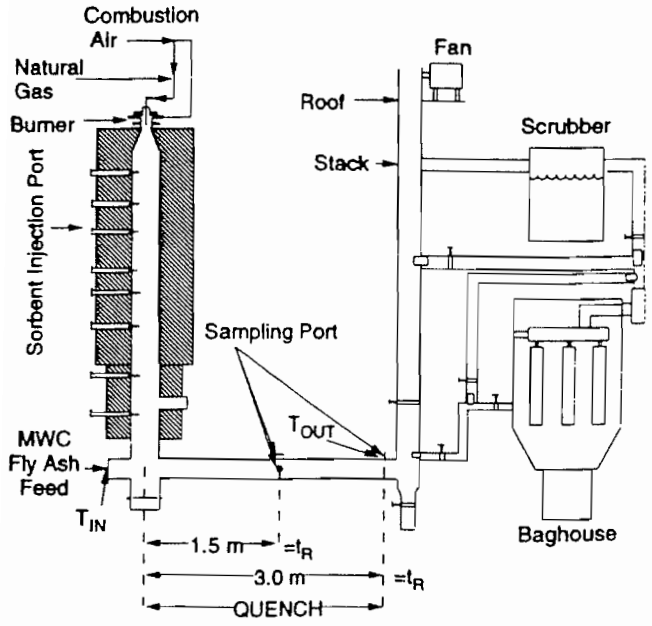

Figure 1. Innovative furnace reactor and sampling locations.

length of the furnace for testing flexibility. The furnace is used to simulate the gaseous combustion environment and quench rate conditions anticipated in MWCs. This is accomplished by doping the fuel with pollutants found in waste combustion, such as HCl. The furnace was operated under nominal conditions with tangential and axial air totaling 0.42 m^3/min STP, including an excess air of 50%.

Experimental Conditions. The flue gas particulate loading of a MWC was simulated by injecting fly ash into the IFR elbow (see Figure 1) from which it passes through the horizontal duct section. Sampling ports are located at the 1.5-m and the 3-m axial locations in the horizontal duct. These sampling ports allow simulation of ≈2 and ≈4 s gas-phase residence times. EPA Modified Method 5 (MM5) sampling trains were installed at each of these sampling locations so as to allow simultaneous sampling at two different residence times for each test. The MWC fly ash sample used for all of the tests was from an ESP hopper on a full-scale (225 Mg/day), mass-burn facility at Quebec City, Canada, prior to facility modifications for improved combustion (*4*). The as-received fly ash was injected through a nozzle with 310 kPa (45 psi) N_2 at 28.3 L/min STP using a calibrated K-Tron feeder at a rate of 100 g/h. This feed rate produced particulate loadings that were representative of those found in conventional mass-burn MWCs upstream of particulate control devices (≈5000 mg/m^3), in addition to producing enough samples for the PCDD and PCDF analytical procedures. Between runs, the horizontal duct section was blown out with high-pressure air to minimize any potential run interactions. The as-received fly ash chemical analysis is shown in Table 1. The fly ash was also analyzed for PCDD and PCDF precursors, such as chlorobenzenes, chlorophenols, and polycyclic aromatic hydrocarbons, but the analytical results consistently showed concentrations below detection limits (200 ng/g). No extractions or treatments were done on the fly ash prior to injection. Since the characteristics of the fly ash are likely significant in determining PCDD and PCDF yields, our work used a single source in order to isolate the effects of combustion and sorbent parameters.

Table 1. Raw Fly Ash Analysis

	PCDD		PCDF	
injected sample	ng/g	ng/Nm³ [a]	ng/g	ng/Nm³
FA1	54.225	270.32	20.799	103.68
FA2	39.493	196.88	16.159	80.55
FA3	38.402	191.44	8.827	44.0
FA4	45.822	228.43	20.625	102.82
FA5	19.506	97.24	8.975	44.74

Ultimate Analysis[b]

moisture, %	1.36
carbon, %	1.08
hydrogen, %	<0.5
Kjeldahl nitrogen, %	0.0094
sulfur, %	3.20
total halogens (calculated as chlorine), %	4.50
ash, %	94.11

Proximate Analysis

moisture, %	1.36
volatile matter, %	3.91
ash, %	94.11
fixed carbon, %	0.62

[a] Based on fly ash mass feedrate and innovative furnace reactor (IFR) duct flow rate. [b] Total may not add to 100% due to analytical methods used for different elements.

Table 2. Test Conditions

run[a]	T_{DUCT} (°C)	QUENCH (°C/s)	t_R (s)	$[O_2]$ (%)	[HCl] (ppm)	$[Cl_2]$ (ppm)	$[Ca(OH)_2]$ (g/min)
1	333.9	34.7	1.87	6.7	0	0	0
2	333.9	34.7	3.74	6.7	0	0	0
3[b]	342.2	34.4	1.93	5.95	0	0	0
5	371.1	38.9	1.87	5.5	0	0	0
6	348.1	36.5	1.79	6.9	0	0	0
7	296.1	21.7	2.11	5.65	0	0	0
8	296.1	21.7	4.23	5.56	0	0	0
10	297.5	31.0	1.9	7.36	0	0	0
12	321.7	34.7	2.44	1.85	0	0	0
14	363.1	41.0	1.67	7.8	0	0	0
16	298.6	32.4	1.77	8.53	100	0	0
17	306.9	31.5	1.7	8.81	1000	0	0
18	311.1	36.1	1.72	8.62	0	30	0
19	312.8	32.8	1.71	8.62	0	300	0
20	303.1	31.8	1.86	7.57	1000	0	2.84
21	338.6	35.7	1.6	8.97	0	0	0
22	353.6	21.5	4.6	2.07	0	0	2.84
23	329.4	16.9	1.51	3.54	1000	300	2.84
24	352.8	23.3	1.91	5.77	0	300	2.84
25	375.8	23.5	4.5	1.73	1000	300	0
26	236.1	31.7	2.08	7.82	0	0	0
27	350.8	40.4	2.26	2.52	0	0	0

[a] Breaks in the numerical sequence result from runs with sampling or analytical problems. Missing runs were repeated for completeness of the test matrix. [b] Indicates run performed at T_{FILT} = 205 °C.

The test matrix was designed to explore the extreme and central parameter values with a view toward applying a second order response surface methodology. Various IFR operating parameters were changed to assess the effect of different combustion and sorbent injection parameters upon downstream PCDD and PCDF formation (the test conditions are listed in Table 2). The temperature of fly ash injection, T_{IN}, at the elbow was varied from 200 to 400 °C by inserting a refractory-embedded cooling coil section upstream of the injection location. The residence time of the fly ash in the duct, t_R, was varied by sampling at different axial locations within the duct and changing volumetric flow rates. The value of t_R was calculated from

the duct volume and flow rate between T_{IN} and point of sampling. Flow rate variation was caused solely by changing the duct temperature, T_{DUCT}, defined as the average of T_{IN} and T_{OUT} (the latter being the duct exit temperature). This difference between T_{IN} and T_{OUT} also was altered and, when divided by the nominal duct transit time (4 s), resulted in varying quench rates, denoted as QUENCH. The temperature of the particulate filter, T_{FILT}, was 205 °C with one run at 120 °C. Clearly, some of these parameters are interrelated, yet all were considered for their mechanistic implications. For example, two runs may have had the same t_R and QUENCH, yet different values of T_{IN}. The oxygen concentration in the duct region, $[O_2]$, was altered by replacing combustion air with N_2. The HCl and Cl_2 concentrations ([HCl] and $[Cl_2]$, respectively) were varied by doping the furnace with premixed cylinder gas. In some tests, sorbent was injected into the IFR at >800 °C at a rate, termed $[Ca(OH)_2]$, of 2.84 g/min. The Ca/Cl stoichiometry was 1.8/1 at 1000 ppm HCl. The sorbent was $Ca(OH)_2$ (D_{50} = 4 μm), commercially available from Tenn Luttrell Co. (Luttrell, TN).

Emissions Sampling. Furnace emissions were sampled in the downstream duct section of the IFR and passed through heated sample lines to continuous emission monitors (CEMs). PCDD and PCDF data are reported in "as-sampled" O_2 and H_2O concentrations. All non-PCDD and non-PCDF gas emission results were corrected to 0% O_2 levels. Gases analyzed for CO_2, O_2, and CO were first passed through a gas dryer and an anhydrous $CaSO_4$ desiccant. All of the above on-line CEMs were zeroed and spanned with gases of known concentration both before and after each daily trial. The downstream Cl concentration was determined by passing a slipstream of the furnace gas through four $Na_2CO_3/NaHCO_3$-filled impingers in an ice bath and by quantifying the impinger catch for Cl^- with ion chromatography.

PCDD and PCDF were sampled at the labeled sampling ports (Figure 1) using isokinetic sampling protocols and EPA MM5 sampling trains. These trains consisted of a quartz sampling probe, followed by a filter, XAD trap, and impingers. The probe rinse, filters, and XAD were analyzed separately, and the results were combined to give a single value for the sampling trains. The water in the impingers was not analyzed.

Sample Analysis. MM5 samples were analyzed by high-resolution gas chromatography/low-resolution mass spectrometry (HRGC/LRMS), using a Hewlett-Packard 5890/5970 gas chromatography/mass selective detector (GC/MSD) system and methods that are slight adaptations of EPA Method 23 (*50*) and RCRA Method 8280 (*51*). Isotopically labeled internal standards for each congener class were incorporated during the extraction and cleanup phases of the analytical procedures to enhance analytical accuracy. For the GC/MSD analyses, the procedures differed from RCRA Method 8280 only in the number of labeled congeners used to calculate recoveries; i.e., congeners containing the 2,3,7,8 substitution positions were avoided as an additional safety precaution. An internal standard was used that consisted of a $^{13}C_{12}$-labeled congener from each tetra--octa-PCDD and -PCDF (except for octa-CDF). The recovery standard $^{6}C_{12}$-labeled TCDD was added before injection on the GC. The recovery had to be within 40–120 % to be acceptable.

Table 3. Total PCDD and PCDF Concentrations[a]

run[b]	measured [PCDD] (ng/Nm³)	predicted [PCDD] (ng/Nm³)	measured [PCDF] (ng/Nm³)	predicted [PCDF] (ng/Nm³)
1	708.87	859	4330.55	3139
2	708.74	859	4574.82	4636
3	877.47	846	5077.91	3902
5	423.53	347	2834.33	3652
6	379.08	593	2322.44	2864
7	1086.19	1170	6578.74	6714
8	1292.32	1170	12508.93	12377
10	1301.79	1033	1278.49	2563
12	43.78	91	296.23	413
14	178.61	53	932.07	1364
16	1067.38	1092	2246.63	1729
17	3266.82	3265	6568.27	6787
18	380.03	382	2342.17	2617
19	1863.14	1863	5207.39	5024
20	279.20	282	680.40	535
21	301.63	275	1151.08	726
22	318.05	318	2592.24	2699
23	300.07	298	1932.17	1951
24	214.45	215	1420.28	1459
25	265.33	265	3193.88	3170
26	55.46	104	9.26	−24
27	447.68	379	1324.93	1078

[a] Based on total of MM5 train (filter, XAD, probe rinse). [b] Breaks in the numerical sequence result from runs with sampling or analytical problems.

Statistical Procedures. The data were initially analyzed using a stepwise regression approach [the STEPWISE option in SAS (*52*) procedure REG] in order to make a tentative decision of the number and identities of the required predictors. The available predictor set consisted of a total of 54 potential predictors including the primary measured parameters $[O_2]$, [HCl], $[Cl_2]$, T_{DUCT}, T_{IN}, T_{OUT}, T_{FILT}, QUENCH, t_R, and $[Ca(OH)_2]$ as well as derived parameters consisting of squares, logarithms, and pairwise products of most of the above. Once a tentative model was attained in this way, then the MAXR option was used to attempt switches among the tentative predictors while looking for an improvement in fit (higher model R^2) within the constraint of maintaining a constant number of predictors. The ultimate criterion for choosing a final model was that all predictors in the model are significant and no other predictor can be added from the excluded list of predictors which attains significance when added to the model. A significance level of $p \leq 0.01$, indicating the probability level that the partial effect of a predictor is significantly different from zero, was chosen as the acceptance criterion. Even though confidence belts reflect statistical precision and were always available, corresponding to the models developed here, we have plotted only those where their addition did not excessively garble the figure's representation of the data.

Results

Table 3 presents the composite yields of tetra- through octa-PCDD and tetra- through octa-PCDF for 22 test runs on the IFR. These yields are calculated from the sum of collected PCDD and PCDF divided by the sampled gas volume. The XAD reported comparatively insignificant PCDD and PCDF yields when compared to the probe catch and filter rinse. Stepwise variable selection, as described above, was used to obtain four optimal empirical models using the parameter units indicated under Nomenclature for predicting yields (in ng/m³) of PCDD, PCDF, the sum

Table 4. Model Predictors

predictor	coefficient	standard error
Section a: [PCDD]		
intercept	−185273.2	21400
ln(O_2 concn)	2816.034051	413
HCl concn	2.525589	0.162
Cl_2 concn	6.927086	0.886
$Ca(OH)_2$ feed rate	−8503.952063	644
duct temp	−117.401381	14.3
ln(duct temp)	38526.234	4490
O_2 × duct temp	−1.740426	0.273
duct temp × $Ca(OH)_2$ feed rate	24.299239	1.94
ln(1 + Cl_2 concn) × res time	−97.011062	16.2
HCl × Cl_2	−0.00430158	0.000881
ln(1 + Cl2 concn) × $Ca(OH)_2$ feed rate	−104.414263	16.0
R^2	0.9810	
MSE	2.22×10^4	
p_{max}	≤0.0006	
Section b: [PCDF]		
intercept	−59138.697	11300
O_2 concn	−2341.91451	366
ln(O_2 concn0	11022.5818	1660
HCl concn	80.537520	8.57
res time	5797.868204	405
ln(duct temp)	9551.920900	1960
duct temp × $Ca(OH)_2$ feed rate	−9.772597	0.770
ln(1 + Cl_2 concn)	681.246152	113.4
quench rate × res time	−144.007661	16.4
duct temp × HCl concn	−0.243753	0.0263
R^2	0.9630	
MSE	5.22×10^5	
p_{max}	≤0.0004	
Section c: [PCDD + PCDF]		
intercept	−161539.1	17800
ln(O_2 concn)	11445.207	1800
HCl concn	110.537338	8.70
res time	6840.432321	406
ln(duct temp)	27304.017	2990
O_2 × duct temp	−7.294521	1.20
duct temp × $Ca(OH)_2$ feed rate	−12.510546	0.783
quench rate × res time	−178.673081	16.3
duct temp × HCl concn	−0.335211	0.0267
ln(1 + Cl_2 concn)^2	159.168549	20.9
R^2	0.9728	
MSE	5.29×10^5	
p_{max}	≤0.0001	
Section d: Logit(φ)		
intercept	−13.410308	1.78
O_2 concn	2.850760	0.251
O_2 × duct temp	$-8.1789985 \times 10^{-3}$	0.000776
quench rate × ln(1 + Cl_2 concn)	−0.014785	0.00238
ln(1 + HCl concn) × res time	−0.043637	0.00964
O_2 concn × res time	−0.043978	0.0150
duct temp × Cl_2 concn	2.42699×10^{-5}	4.12×10^{-6}
duct inlet T	0.029135	0.00441
R^2	0.9499	
MSE	0.06469	
p_{max}	≤0.0005[a]	

[a] $p = 0.0110$ for O_2 concn × res time.

of PCDD and PCDF, and the logit of PCDD, termed [PCDD], [PCDF], [PCDD + PCDF], and logit(φ), respectively. Logit (φ) is defined by

$$y = \text{logit}(\varphi) = \log_e\left[\frac{\varphi}{(1-\varphi)}\right] \quad (2)$$

where φ = [PCDD]/[PCDD + PCDF], representing the partition coefficient between [PCDD] and [PCDF]. Use of the logit transform enables statistical analysis while numerically constraining φ to [0,1]. For each model, Table 4 lists an estimated regression coefficient for each significant predictor in the model and its standard error. A response can be predicted by forming the appropriate weighted linear combination of the predictors, using the regression weights as shown, and then adding the indicated intercept. φ can be calculated from logit(φ) by performing the inverse transform

$$\varphi = [1 + \exp(-y)]^{-1} \quad (3)$$

Table 5. Contributions of Parameters

parameter	semipartial correlation
Section a: [PCDD]	
oxygen concn	0.0914
HCl concn	0.4931
Cl_2 concn	0.2510
$Ca(OH)_2$ feed rate	0.5670
duct temp	0.3902
res time	0.0679
Section b: [PCDF]	
oxygen concn	0.2400
HCl concn	0.2850
Cl_2 concn	0.1113
$Ca(OH)_2$ feed rate	0.4966
duct temp	0.4989
res time	0.7164
quench rate	0.2390
Section c: [PCDC + PCDF]	
oxygen concn	0.0923
HCl concn	0.3799
Cl_2 concn	0.1312
$Ca(OH)_2$ feed rate	0.5774
duct temp	0.6139
res time	0.6990
quench rate	0.2710
Section d: Logit(φ)	
oxygen concn	0.5822
HCl concn	0.0733
Cl_2 concn	0.1391
duct temp	0.3998
res time	0.1095
quench rate	0.1376
inlet temp	0.1561

All retained predictors were quite significant ($p \leq 0.0007$, with the exception of $[O_2]t_R$ in the logit model), while $R^2 \geq 0.950$ indicated that a major fraction of the variation of each of the responses was explained by variation of its associated predictor set. Table 5 summarizes the primary predictors required for each of the models and lists their semipartial correlations, R^2_{SP}, as a means of quantifying their relative importance. The $R^2_{SP}(P, ...)$ values represent the fraction of the variance of the response variable (such as [PCDD]) attributable to variation in a particular parameter, P [through all predictors containing P in its various forms, denoted by $(P, ...)$], while holding all of the other parameters constant (*52*). As such, their values are somewhat dependent on the range over which the specific parameter is varied; for example, variation of t_R from 1.00 to 1.01 s is unlikely to have a strong effect on yield and therefore would probably result in a low value of $R^2_{SP}(t_R, ...)$. We chose to vary the range of each parameter over reasonably expected field values. In this manner, our derived values of R^2_{SP} should adequately reflect actual mechanistic importance.

The predictor sets for [PCDD] and [PCDF] showed four correspondences among 11 and 9 predictors, respectively, and greater correspondence with the set that determines [PCDD + PCDF]. However, a relatively distinct predictor set determined composition. Only one correspondence was found with the predictor set which

Table 6. Ability of Models To Predict Other Response Variables

	[PCDD]	[PCDF]	[PCDD + PCDF]	logit(φ)
[PCDD]	0.9807	0.6518	0.7468	0.7995
[PCDF]	0.7499	0.9628	0.9624	0.7871
[PCDD + PCDF]	0.7732	0.9563	0.9727	0.7594
logit(φ)	0.2450	0.5267	0.4549	0.9501

determined logit(φ) and those of all three other models. The distinction between the yield and composition models is emphasized further by Table 6 which lists R^2 when each of the selected models is used to predict the other three response variables. Yield models for [PCDD], [PCDF], or [PCDD + PCDF] predicted the partition coefficient or logit(φ) reasonably well (i.e., $R^2 \approx 0.8$), but the optimal model for logit(φ) composition was a very poor predictor of the three yield models.

The ability of the models to predict the actual results is shown in Table 3. The high level of agreement between actual and predicted values demonstrates the models' predictive capabilities. Table 4 also reports mean squared error (MSE) as an estimate of replication variance. The square root of MSE estimates the standard deviation of an individual observation.

Model Sensitivity Analyses

The predictors from the four models can be used to determine the influence of each parameter in predicting yield through examination of

$$\partial[\text{yield}]/\partial(\text{parameter}) \qquad (4)$$

This will indicate the extent to which that rate is affected by variation and interaction of the test parameters within the tested range. The following discussion examines the experimental parameters $[O_2]$, [HCl], $[Cl_2]$, T_{DUCT}, T_{IN}, T_{OUT}, T_{FILT}, QUENCH, t_R, and $[Ca(OH)_2]$ in this manner. For illustrative purposes, this analysis is fully developed for the $[O_2]$ parameter. Subsequent discussions on other parameters will focus on only the most significant predictors, as reflected by higher values of R^2_{SP} (from Table 5).

Oxygen Concentration. [PCDD + PCDF] is described by two O_2-related predictors, ln $[O_2]$ and the interactive term of $[O_2]T_{DUCT}$ (Table 4 section c). However, even the combined effect of these two predictors has a low $R^2_{SP}(O_2, ...)$ (0.0923, Table 5, section c), indicating that the effect of $[O_2]$ in explaining [PCDD + PCDF] variation under our test conditions is minimal and can be better explained by other experimental parameters. Nonetheless, Table 4, section c can be used to explain the effect of $[O_2]$ on [PCDD + PCDF] yield. The rate of [PCDD + PCDF] change with respect to changes in $[O_2]$ can be described by the partial derivative of the appropriate weighted linear combination of the predictors. Since

$$[\text{PCDD + PCDF}] = 11445.2 \ln[O_2] - 7.3[O_2]T_{DUCT} + f([\text{HCl}], [Ca(OH)_2], t_R, \text{QUENCH}, [Cl_2]) \qquad (5)$$

the partial derivative is

$$\frac{\partial[\text{PCDD + PCDF}]}{\partial[O_2]} = \frac{11445.2}{[O_2]} - 7.3T_{DUCT} \qquad (6)$$

implying that [PCDD + PCDF] will increase with increases in $[O_2]$ if and only if eq 6 is greater than zero, or when

$$[O_2] < \frac{11445.2}{7.3T_{DUCT}} \approx \frac{1570}{T_{DUCT}} \qquad (7)$$

Where strict equality holds, changes in $[O_2]$ will have no effect upon [PCDD + PCDF] yield (this is the region of maximum [PCDD + PCDF]). Figure 2 shows this interactive effect of $[O_2]$ and T_{DUCT} on [PCDD + PCDF] at T_{DUCT} values of 252 and 379 °C with other parameters set at typical values. Clearly, there is a dividing line in the $[O_2]T_{DUCT}$ plane at which further increases in $[O_2]$ result in reductions of [PCDD + PCDF]. As seen in the figure, this occurs at intermediate values of $[O_2]$.

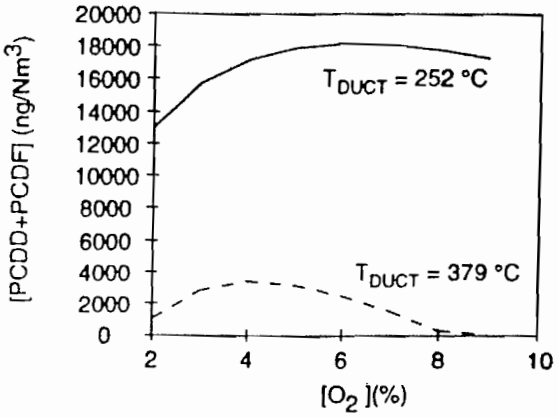

Figure 2. Effect of $[O_2]$ on [PCDD + PCDF] at two values of T_{DUCT} ([HCl] = 500 ppm, $[Cl_2]$ = 30 ppm, $[Ca(OH)_2]$ = 0 g/min, t_R = 1.7 s, QUENCH = 24 °C/s).

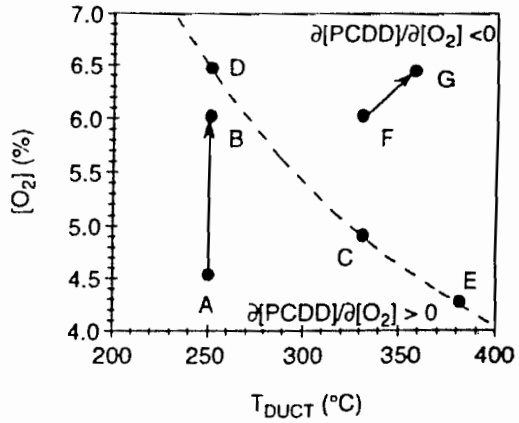

Figure 3. Effect of T_{DUCT} and $[O_2]$ on $\partial[\text{PCDD}]/\partial[O_2]$. The dashed line indicates where $\partial[\text{PCDD}]/\partial[O_2] = 0$.

The effect of $[O_2]$ on predicting [PCDD] is not particularly significant. Table 5, section a shows $R^2_{SP}(O_2, ...)$ to be 0.0914. As above, it is described by ln $[O_2]$ and $[O_2]T_{DUCT}$ predictors. Evaluation of $\partial[\text{PCDD}]/\partial[O_2]$ indicates that as long as

$$[O_2] < \frac{2816.03}{1.7404T_{DUCT}} \approx \frac{1620}{T_{DUCT}} \qquad (8)$$

this rate will be positive, meaning that increases in $[O_2]$ will result in increased [PCDD]. Otherwise, increases in $[O_2]$ will result in decreased [PCDD]. The $[O_2]$ corresponding to the maximum [PCDD] decreases with increasing T_{DUCT}. These results are graphically displayed in Figures 3 and 4. For example, operating conditions at point A are in a region in which increases in $[O_2]$ will result in increased [PCDD]. Changing operating condi-

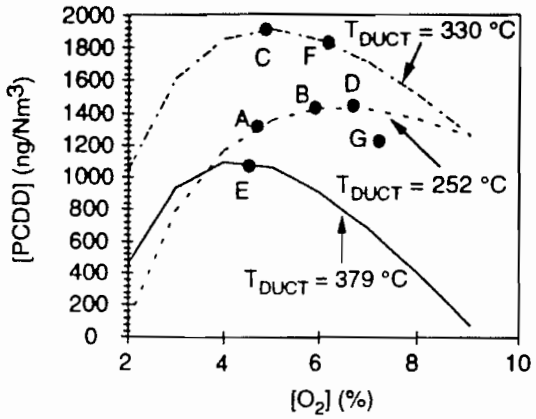

Figure 4. Effect of $[O_2]$ on [PCDD] at three values of T_{DUCT} ([HCl] = 500 ppm, $[Cl_2]$ = 30 ppm, $[Ca(OH)_2]$ = 0 g/min, t_R = 1.7 s, QUENCH = 24 °C/s).

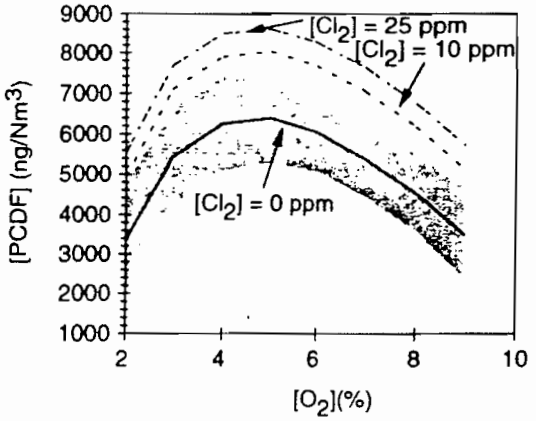

Figure 5. Effect of $[O_2]$ on [PCDF] at three values of $[Cl_2]$ ([HCl] = 500 ppm, $[Ca(OH)_2]$ = 0 g/min, t_R = 1.7 s, QUENCH = 24 °C/s). The shaded area represents the 95% confidence interval.

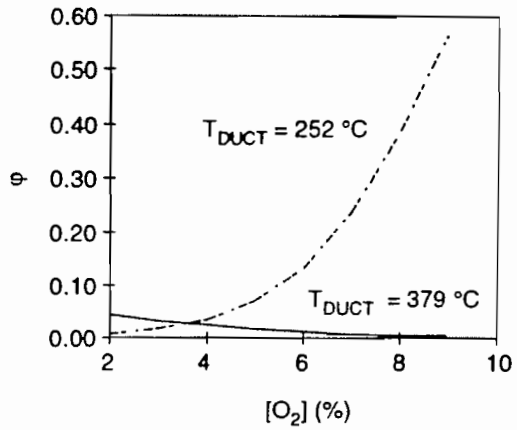

Figure 6. Effect of $[O_2]$ on φ at two values of T_{DUCT} ([HCl] = 500 ppm, $[Cl_2]$ = 30 ppm, $[Ca(OH)_2]$ = 0 g/min, t_R = 1.7 s, QUENCH = 24 °C/s).

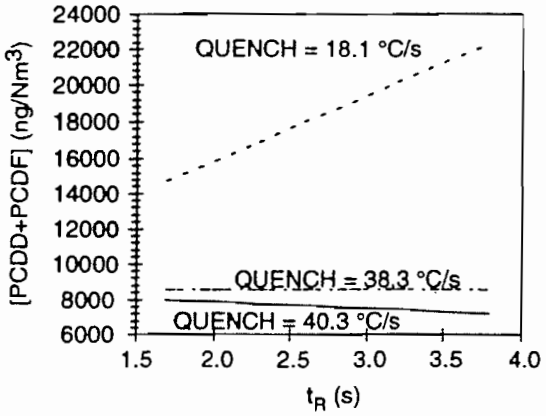

Figure 7. Effect of t_R on [PCDD + PCDF] at three values of QUENCH ([HCl] = 500 ppm, $[Cl_2]$ = 30 ppm, $[Ca(OH)_2]$ = 0 g/min, $[O_2]$ = 6%, T_{DUCT} = 299 °C).

tions from point A to point B will result in decreased sensitivity of [PCDD] with respect to changes in $[O_2]$, although the rate of [PCDD] per change in $[O_2]$ will still be positive. Changes from point C to points D or E have no effect on the rate of [PCDD] formation with changes in $[O_2]$, ∂[PCDD]/$\partial[O_2]$, although the second derivative of the yield equation indicates that this domain is in the region of maximum [PCDD] yield for that particular T_{DUCT}. Point F is in a region in which increased $[O_2]$ will result in decreased [PCDD] yield, and moving from point F to point G will further increase the rate at which higher $[O_2]$ results in declining [PCDD].

[PCDF] yield is determined by two O_2 predictors. Although $[O_2]$ is a more significant predictor than in the above two models [$R^2_{SP}(O_2, ...)$ is 0.2400, Table 5, section b], four other parameters have a stronger predictive effect on [PCDF]. [PCDF] increased with increasing $[O_2]$ at a rate $-2341.91 + 11022.58/[O_2]$ ng m^{-3} %$^{-1}$ so long as $[O_2] \leq 11022.58/2341.91 = 4.7\%$, and decreased thereafter.

Figure 5 shows the effect of $[O_2]$ and $[Cl_2]$ on [PCDF] formation. Note that for any $[O_2]$, ∂[PCDF]/$\partial[O_2]$ is not affected by $[Cl_2]$ (the curves are all parallel). Maximum [PCDF] occurs at 4.7% $[O_2]$, and any increases in $[Cl_2]$ result in greater [PCDF]. The shaded area indicates the 95% confidence interval for the $[Cl_2]$ = 0 ppm case.

Logit(φ) increased with increasing $[O_2]$ at a rate [2.8508 − 0.008180 T_{DUCT} − 0.04398 t_R] logit units/% so long as the term in square brackets is positive; i.e., for low T_{DUCT} and/or short t_R. This result is illustrated by Figure 6. Clearly, there is a dividing line in the $T_{DUCT}t_R$ plane beyond which the logit(φ) decreases with increasing $[O_2]$.

The high $R^2_{SP}(O_2, ...)$ for logit(φ) (0.5822, Table 5, section d) indicates that O_2 is a strong parameter in determining whether formation of PCDD or formation of PCDF is favored. Increases in $[O_2]$ will favor PCDD formation over PCDF, although higher T_{DUCT} and t_R will temper this effect. Since the toxic equivalency of PCDD isomers is 1–10 times that of PCDF isomers (*53*), operational measures to decrease logit(φ) may reduce health and environmental risks.

Quench Rate. All four models do not indicate QUENCH as a very significant parameter in describing yield (as seen in Table 5), although QUENCH is more significant than $[O_2]$. Indeed, QUENCH is never a significant predictor for [PCDD]. Determination of partial derivatives of yield with respect to QUENCH (as for $[O_2]$ above) shows that, for all three other models, the effect of QUENCH is such that increases in QUENCH always decrease yield. This effect becomes more dramatic as t_R increases for [PCDD + PCDF] and [PCDF], as can be seen for the former in Figure 7.

Residence Time. t_R is a predictor for all four models; however, its overall effect is most significant in describing [PCDD + PCDF] [$R^2_{SP}(t_R, ...)$ = 0.6990, Table 5, section c] and [PCDF] [$R^2_{SP}(t_R, ...)$ = 0.7164, Table 5, section b]. Indeed, $R^2_{SP}(t_R, ...)$ is the single most significant parameter in these two models. ∂[PCDD + PCDF]/∂t_R increased as long as QUENCH ≤ 38 °C/s (101 °F/s), as shown in Figure

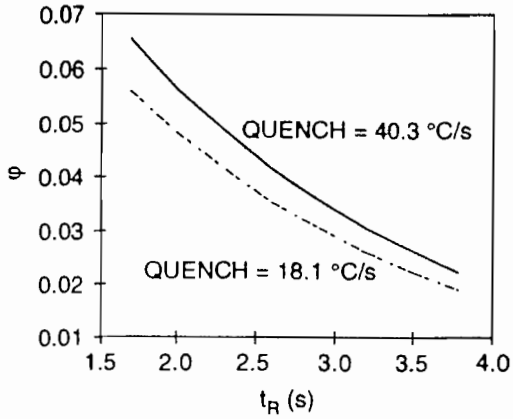

Figure 8. Effect of t_R on φ at two values of QUENCH ([HCl] = 500 ppm, $[Cl_2]$ = 30 ppm, $[Ca(OH)_2]$ = 0 g/min, $[O_2]$ = 6%, T_{DUCT} = 299 °C).

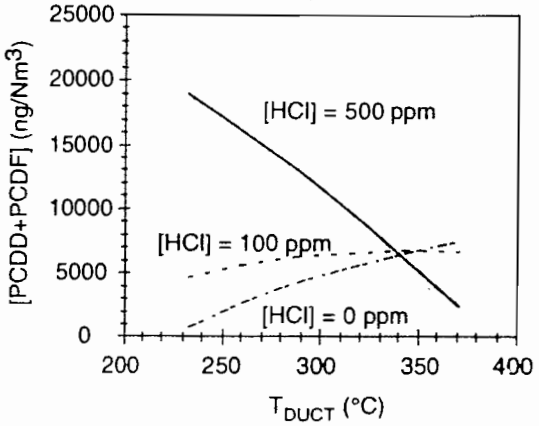

Figure 9. Effect of T_{DUCT} on [PCDD + PCDF] at three values of [HCl] ($[Cl_2]$ = 30 ppm, $[Ca(OH)_2]$ = 0 g/min, $[O_2]$ = 6%, t_R = 1.7 s, QUENCH = 28 °C/s). The shaded area represents the 95% confidence interval.

7. Greater values of QUENCH resulted in decreased formation of [PCDD + PCDF]. Increases in t_R lower the PCDD fraction, as shown in Figure 8 by declining values of φ at longer times. Variation of QUENCH has a relatively minor affect upon φ.

Duct Temperature. T_{DUCT} is a significant predictor for all four models, although it is most significant in describing [PCDD + PCDF] [$R^2_{SP}(t_R, ...)$ = 0.6139, Table 5, section c] and [PCDF] [$R^2_{SP}(t_R, ...)$ = 0.4989, Table 5, section b].

[PCDD + PCDF] is described by four predictors containing T_{DUCT}. The rate ∂[PCDD + PCDF]/∂T_{DUCT} will decrease as T_{DUCT} gets higher (as seen by the barely discernible drop in slopes of the three curves on Figure 9) and will decline more rapidly with increases in $[O_2]$, $[Ca(OH)_2]$, and [HCl]. A sufficiently high value of $[O_2]$, $[Ca(OH)_2]$, or [HCl] will make ∂[PCDD + PCDF]/∂T_{DUCT} become negative, resulting in declining [PCDD + PCDF]. This is shown in Figure 9 with increasing values of [HCl] up to 500 ppm.

The term ∂[PCDF]/∂T_{DUCT} is likewise decreased by increasing T_{DUCT}, $[Ca(OH)_2]$, and [HCl] while ∂[PCDD]/∂T_{DUCT} decreases by increasing T_{DUCT} or increasing $[O_2]$, but increases with increasing $[Ca(OH)_2]$.

The logit(φ) model is always negatively affected by increases in T_{DUCT}. Higher values of T_{DUCT} will therefore decrease the [PCDD] compared to [PCDF].

Effect of HCl Concentration. [HCl] is a significant parameter, being included in predictors for all four models.

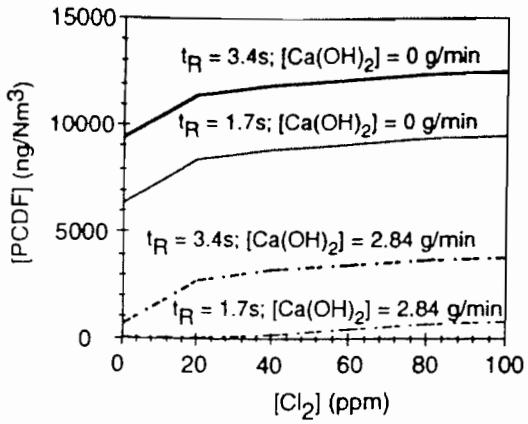

Figure 10. Effect of $[Cl_2]$ on [PCDF] at two values of $[Ca(OH)_2]$ and t_R ([HCl] = 100 ppm, $[O_2]$ = 6%, T_{DUCT} = 315.6 °C, t_R = 1.7 and 3.4 s, QUENCH = 28 °C/s).

It is most significant in describing [PCDD] [R^2_{SP}(HCl, ...) = 0.4931] and [PCDD + PCDF] [R^2_{SP}(HCl, ...) = 0.3799] in Table 5, sections a and c, respectively, while less significant in explaining logit(φ) [R^2_{SP}(HCl, ...) = 0.0733].

The effect of increases in [HCl] is to increase ∂[PCDD + PCDF]/∂[HCl] at a rate of [110.5 - 0.3352 T_{DUCT}] ng m^{-3} ppm^{-1}. Thus, as long as T_{DUCT} is less than 330 °C (626 F), our results show increased [PCDD + PCDF] with increases in [HCl]. Above this temperature, increases in [HCl] will result in lower [PCDD + PCDF]. This is shown on Figure 9 by the cross-over of the concentration plots.

Increases in [HCl] always led to increases in [PCDD], within the range of our data and model. This should hold for $[Cl_2] \leq 100$ ppm, which should always be the case in field operations.

Effect of Cl_2 Concentration. $[Cl_2]$ is a significant predictor for all four models, although it appears to have less of an influence (lower R^2_{SP}) than [HCl] except for logit(φ). Note, however, that this may only reflect the envelope of experimental conditions chosen. Four Cl_2-related predictors are included in the [PCDD] model, which reports the highest $R^2_{SP}(Cl_2, ...)$ of the four models, or 0.2510 (Table 5, section a). Increases in t_R, [HCl], and $[Ca(OH)_2]$ will lower the rate at which ∂[PCDD]/$\partial[Cl_2]$ increases with increasing $[Cl_2]$. It is also worth noting that ∂[PCDF]/$\partial[Cl_2]$ is always nonnegative; increases in $[Cl_2]$ always produce higher [PCDF], albeit at a declining rate. The combined effects of t_R, $[Cl_2]$, and $[Ca(OH)_2]$ on [PCDF] are shown in Figure 10. Increased [PCDF] is observed with increasing $[Cl_2]$ and t_R while the addition of $Ca(OH)_2$ sorbents showed significant decreases.

Effect of $Ca(OH)_2$. The presence of $Ca(OH)_2$ is one of the most important parameters in describing [PCDD], [PCDF], and [PCDD + PCDF] as indicated by their R^2_{SP}-$[Ca(OH)_2, ...]$ (0.5670, 0.4966, and 0.5774, respectively). Interestingly, $[Ca(OH)_2]$ is not included as a predictor for describing the partition between PCDD and PCDF.

The effect of sorbent addition is seen collectively in Figures 10–12 along with concurrent effects of other selected parameters. Figure 11 shows that addition of $Ca(OH)_2$ sorbent significantly reduces [PCDD + PCDF] yield at all values of T_{DUCT}. On the basis of our choice of parameters in Figure 11, when T_{DUCT} > 315 °C, the addition of $Ca(OH)_2$ reduces the yield to zero. Since ∂[PCDD + PCDF]/$\partial[Ca(OH)_2] \propto -T_{DUCT}$ (see Table 4, section c) and T_{DUCT} is never negative, the addition of $Ca(OH)_2$ will always decrease [PCDD + PCDF]. The

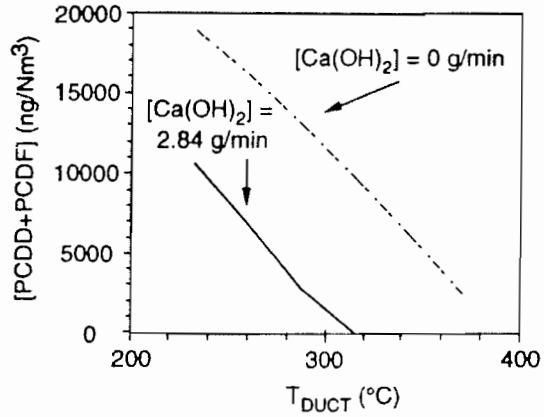

Figure 11. Effect of T_{DUCT} on [PCDD + PCDF] at two values of [Ca(OH)$_2$] ([HCl] = 500 ppm, [Cl$_2$] = 30 ppm, [O$_2$] = 6%, t_R = 1.7 s, QUENCH = 28 °C/s).

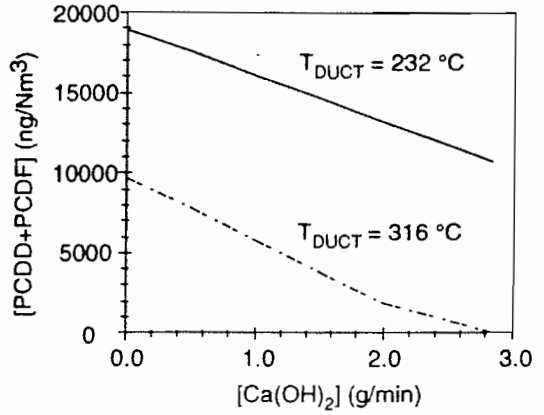

Figure 12. Effect of [Ca(OH)$_2$] on [PCDD + PCDF] at two values of T_{DUCT} ([HCl] = 500 ppm, [Cl$_2$] = 30 ppm, [O$_2$] = 6%, QUENCH = 28 °C/s, t_R = 1.7 s).

incremental effect of sorbent addition at two values of T_{DUCT} is shown in Figure 12.

The model for [PCDD] is more complicated. In the absence of Cl_2, [PCDD] decreases everywhere with the addition of $Ca(OH)_2$ except when T_{DUCT} is ≥350 °C (662 F). If [Cl$_2$] is nonzero (as in most realistic cases), this minimum temperature will increase.

The effect of [Ca(OH)$_2$] on [PCDF] is the same as with [PCDD + PCDF]. Addition of $Ca(OH)_2$ will always lead to reduction in [PCDF] since T_{DUCT} is always non-negative.

The model logit(φ) is not described by any predictor terms containing [Ca(OH)$_2$].

Other Parameters. Additional parameters of T_{IN}, T_{OUT}, and T_{FILT} were considered. Of these parameters, only T_{IN} met the predictor criterion. The model for logit(φ) has T_{IN} as a predictor, although $R^2_{SP}(T_{IN}, ...)$ is low. The lack of significance of T_{FILT} suggests that there is no significant difference between yields from sampling filters at 205 °C versus 120 °C. This resolves a concern that yields are artificially high due to further reaction on the 205 °C filter.

Discussion

Significant increases in [PCDD] and [PCDF] (over 2 orders of magnitude) can be found in comparing the initial, raw fly ash concentrations in Table 1 with that of the tested fly ash in Table 3. This indicates that PCDD and PCDF formation occur at low T_{DUCT} [≤376 °C (708.5 F)] and short t_R (<4.6 s), validating long-standing findings of postfurnace, downstream PCDD and PCDF formation. It also suggests that collected ESP fly ash is still active for formation and that sufficient organic precursors are present (either on the fly ash or in the natural gas combustion products) to form PCDD and PCDF. Tests without the addition of Cl as HCl or Cl_2 also show large increases in PCDD and PCDF, indicating that sufficient Cl precursors are also present on the fly ash to produce PCDD and PCDF. These findings are consistent with both the chloro-organic percursor (*6, 17*) and *de novo* (*15*) hypotheses.

The volumetric concentrations of sampled PCDD and PCDF are, in many cases, several times higher than those obtained from field sampling trials on MWCs prior to flue gas cleaning equipment and without "good combustion practices" (GCPs). The facility from which the fly ash used in these tests was obtained had PCDD + PCDF levels up to 4000 ng/Nm^3 prior to GCP facility modifications (*4*). GCPs typically include appropriate temperature control, air rates and distribution, and boiler structure modifications to improve mixing (*54*). The higher concentrations sometimes found in our work are likely due to any number of factors inherent in our simulation of a MWC. These might include a higher percentage of condensed organics on our collected fly ash than is representative of *in situ* fly ash.

The time rate of PCDD and PCDF formation reached a maximum of 1160 ng (g of fly ash)$^{-1}$ s^{-1} in run 17. This rate is apparently the highest value reported to date from an experimental system. Rate results from bench-top, fixed bed reactors have been typically more than 2 orders of magnitude less with the exception of recent results with a PCP precursor [147 ng (g of fly ash)$^{-1}$ s^{-1}, (*19*)]. Even this recent result requires a mechanism including particle deposition for sufficient residence time, reaction, and subsequent reentrainment or desorption to explain some field-observed (*34*) PCDD and PCDF concentrations. The rate of PCDD and PCDF formation observed in our work suggests that in-flight formation alone is sufficiently rapid to explain concentrations observed in field-scale operations.

The effect of [O$_2$] over the range of our experiments was minimal except in determining the partition coefficient between [PCDD] and [PCDF]. [O$_2$] had a high value of $R^2_{SP}(O_2, ...)$ (0.5822) for logit(φ) and, as such, is the most influential parameter in determining the partitioning between PCDD and PCDF. Increases in [O$_2$] will lead to greater fractions of the yield as PCDD, as shown on Figure 6, if T_{DUCT} is sufficiently low. High values of T_{DUCT} always lead to low values of logit(φ) while lower T_{DUCT} requires low [O$_2$] (<5%) to achieve comparable values of φ (Figure 6). In general, [O$_2$] values at the extremes (<3% or >7%) of the range of our operating conditions tended to produce lower [PCDD + PCDF] (Figure 2). This may reflect a combination of two phenomena: (1) as [O$_2$] increases, the production of [Cl$_2$] via eq 1 may wane as [HCl] or catalyst reactivity becomes limiting (as in ref 29) and (2) at low [O$_2$], a dechlorination/hydrogenation reaction might occur (*14*).

Increases in fly ash t_R have a significant effect upon [PCDF] and [PCDD + PCDF] (the latter is shown in Figure 7) as long as QUENCH is less than 40 and 38 °C/s, respectively. At values of QUENCH approaching or exceeding these values, additional residence time does not have a particularly significant impact upon yields. Slow

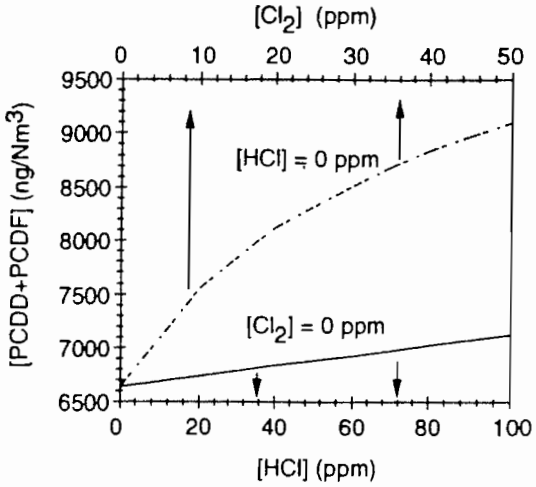

Figure 13. Effect of equimolar [HCl] and [Cl_2] on [PCDD + PCDF] ([$Ca(OH)_2$] = 0 g/min, [O_2] = 6%, T_{DUCT} = 315 °C, QUENCH = 24 °C/s, t_R = 1.7 s).

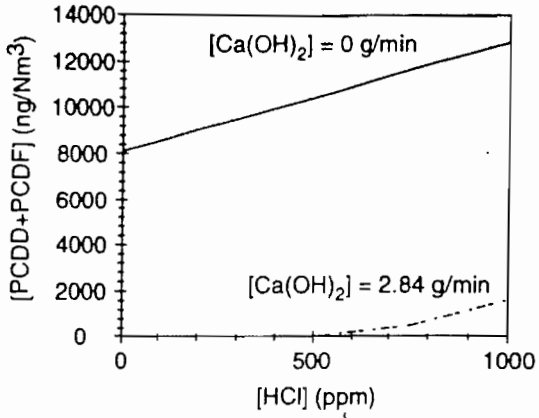

Figure 14. Effect of [HCl] on [PCDD + PCDF] with and without [$Ca(OH)_2$] (O_2 = 6%, Cl_2 = 20 ppm, $Ca(OH)_2$ = 0 and 2.84 g/min, t_R = 1.7 s, T_{DUCT} = 315 °C, QUENCH = 24 °C/s).

flue gas cooling is a condition favorable to [PCDF] formation, in apparent agreement with others' results (*32*). Higher values of QUENCH result in decreased formation as seen in Figure 7 where [PCDD + PCDF] drops dramatically as QUENCH is increased from 18 to 38 °C/s. The dependence of [PCDD + PCDF] on QUENCH at a given t_R suggests that yields are related to the amount of time that the reactants remain in an optimal temperature region.

The partial effect of additional HCl and Cl_2 (varying HCl and Cl_2 while holding constant all other parameters) is, within statistical limits, always to increase dramatically the levels of PCDD and PCDF from those of undoped baseline runs. Thus, both on-particle Cl and gaseous Cl lead to increased yields, although the yield from the latter is generally over twice that of the former. Earlier work (*25*) showed that Cl_2 was more apt to chlorinate organic precursors than HCl. Our model results suggest that this is true as long as [Cl_2] is within the expected field values and T_{DUCT} is above ≈270 °C. Figure 13 compares [PCDD + PCDF] from equimolar Cl values of [HCl] and [Cl_2]. [PCDD + PCDF] is much higher from Cl_2 than HCl, supporting our earlier findings.

The relative inability of [HCl] to affect [PCDD + PCDF] at $T_{DUCT} \geq 330$ °C in the presence of 30 ppm [Cl_2] (Figure 9) suggests that formation at the higher temperatures is limited by another step in the mechanism or proceeds by a different mechanism, perhaps reaction with Cl present on the injected fly ash.

[$Ca(OH)_2$] was the most influential parameter in determining the sampled values of [PCDD], [PCDF], and [PCDD + PCDF], although it had no effect upon determining the partitioning between PCDD and PCDF, as reflected by φ. Injection of $Ca(OH)_2$ sorbent at a temperature >800 °C significantly reduced [PCDD + PCDF] (see Figure 14). This is true even during the "baseline" runs when no additional Cl source was added. The presence of $Ca(OH)_2$ reduces the yields expected from formation on particle surfaces where the only source of Cl is that which is found on the fly ash feed. These results also show that $Ca(OH)_2$ interferes with formation on the particle itself, reducing PCDD and PCDF yields beyond those expected from gaseous HCl removal alone. At T_{DUCT} ≈280 °C (all but run 26), the presence of $Ca(OH)_2$ has an inhibitory effect upon [PCDD + PCDF] beyond that attributable to reduction in gas-phase [HCl] alone (injection of 2.84 g/min typically drops [HCl] ≈70%). [PCDD + PCDF] with [$Ca(OH)_2$] = 2.84 g/min is much lower than for the equivalent [HCl] (300 ppm) with no added [$Ca(OH)_2$].

Table 5 suggests that, after [$Ca(OH)_2$], T_{DUCT} is the most significant parameter in describing [PCDD], [PCDF], and [PCDD + PCDF]. In addition, after [O_2], T_{DUCT} also is the second most significant parameter in describing logit-(φ). The results suggest that, in general, under normal operating conditions lower values of [PCDD], [PCDF], and [PCDD + PCDF] are found at higher values of T_{DUCT}, ≈>350 °C. This may, however, be somewhat of an artifact from the manner in which the samples were collected. The runs with high T_{DUCT} were in part due to their association with high values of T_{OUT}, the latter being within the commonly cited temperature region of PCDD and PCDF formation (300–400 °C). Thus, these samples may still have been undergoing appreciable reaction at the point (temperature) of sampling, resulting in lower amounts of collected PCDD and PCDF and, therefore, in being associated with higher values of T_{DUCT}. This phenomenon combines with [HCl] in Figure 9 to show lower [PCDD + PCDF] values at higher [HCl]. These results suggest that the formation mechanism shifts with temperature. For instance, surface-bound Cl on fly ash may be more active at higher temperatures, while gaseous HCl does not play a significant role until lower temperatures are reached.

The partition coefficient, φ, is least affected by parameters related to Cl composition ([HCl], [Cl_2], [$Ca(OH)_2$]) but is rather almost solely affected by the parameters T_{DUCT} and [O_2]. Figure 6 shows that lower [O_2] and higher T_{DUCT} result in lower values of φ, meaning less [PCDD] in relation to [PCDF]. This suggests that formation of PCDD versus PCDF requires higher amounts of O_2 and lower temperatures. The role of O_2 in PCDD formation from particulate carbon has been noted earlier (*18*) and is likely due to the O dependency of both the Deacon reaction (eq 1) and the phenol (a PCDD precursor) formation.

Conclusions

In-flight formation of PCDD and PCDF to levels representative of those observed in field sampling trials has been observed by reinjection of MWC fly ash and downstream sampling in a pilot-scale combustor. Formation of PCDD and PCDF to field-representative levels

can be explained sufficiently by a mechanism that involves reaction on an entrained particle at residence times less than 5 s.

System parameters that significantly affect the PCDD:PCDF partitioning include $[O_2]$ and T_{DUCT}. This suggests that measures could be taken to control this partitioning, rather than the total yield of PCDD and PCDF, to effect the greatest reduction in health and environmental toxicity.

Combustion modifications that lead to changes in the operating characteristics of the duct environment can result in reduced PCDD and PCDF formation. At high values of QUENCH, t_R has little influence on yields. The converse is true at lower values of QUENCH, implying that more rapid quench rates in the duct system will result in lower PCDD and PCDF yields. In a related manner, higher average duct temperatures result in less formation of PCDD and PCDF. While $[O_2]$ did not have a strong correlation with levels of PCDD or PCDF formation, variation of excess air still has an effect on yields; its significance was most prominent in explaining the partitioning between PCDD and PCDF. Intermediate levels of $[O_2]$ (≈4–7 %) tend to produce larger PCDD and PCDF yields than the extremes.

The presence of high temperature (>800 °C) $Ca(OH)_2$ sorbent injection has a significant role in preventing PCDD and PCDF formation. The resultant reductions in the HCl or Cl_2 concentrations, especially at lower values of T_{DUCT}, significantly decrease the formation of PCDD and PCDF. Sorbent addition, even in the absence of added gaseous Cl species, reduces PCDD and PCDF yields, implying suppression of a mechanism involving particle-bound Cl.

The effect of combustor operating parameters on PCDD and PCDF yield during waste combustion is interactive, resulting in complicated interrelationships. This underscores the difficulties in drawing mechanistic conclusions from parametrically uncontrollable field tests. Despite their complexity, these pilot-scale results can be used to begin to understand the effect of sorbent injection and combustion operating conditions upon PCDD and PCDF yields and suggest the means for minimizing the potential for downstream formation of PCDD and PCDF.

Nomenclature

logit(φ)	[PCDD] fraction of total yield, defined in eq 2
D_{50}	median particle diameter, μm
QUENCH	temperature quench rate, °C/s
R^2	model coefficient of determination, unitless
$R^2_{SP}(P, ...)$	semipartial correlation of the model set of predictors including parameter P, unitless
T_{DUCT}	temperature of the duct, °C
T_{FILT}	temperature of the particulate filter, °C
T_{IN}	temperature at fly ash injection point, °C
T_{OUT}	temperature at sampling point, °C
t_R	gas- and particle-phase residence time, s
$[Ca(OH)_2]$	concentration of $Ca(OH)_2$, g/min
$[Cl_2]$	concentration of Cl_2, ppmv
[HCl]	concentration of HCl, ppmv
$[O_2]$	concentration of O_2, %
[PCDD + PCDF]	total yield of [PCDD] and [PCDF], ng/m³
[PCDD]	yield of [PCDD], ng/m³
[PCDF]	yield of [PCDF], ng/m³
φ	[PCDD]/[PCDD + PCDF], unitless
y	logit(φ), defined in eq 2

Acknowledgments

The authors gratefully acknowledge the field-related information from James D. Kilgroe (U.S. EPA/AEERL); the mechanical support of George R. Gillis (U.S. EPA/AEERL); the sampling efforts of C. Courtney, A. Drago, W. Hansen, and R. Srivistava (Acurex Environmental); and the analytical efforts of R. Harris, B. Harrison, and J. Ryan (Acurex Environmental).

Literature Cited

(1) Shaub, W.; Tsang, W. *Environ. Sci. Technol.* **1983**, *17*, 721–730.
(2) Shaub, W.; Tsang, W. Physical and chemical properties of dioxins in relation to their disposal. In *Human and Environmental Risks of Chlorinated Dioxins and Related Compounds*; Tucker, R. E., Young, A. L., Gray, A., Eds.; Plenum Press: New York, 1983; pp 731–748.
(3) Commoner, B.; Shapiro, K.; Webster, T. *Waste Manage. Res.* **1987**, *5*, 327–346.
(4) Environment Canada. *Environmental Characterization of Mass Burning Incinerator Technology at Quebec City*; Summary Report; National Incinerator Testing and Evaluation Program: Ottawa, June 1988; EPS 3/UP/5.
(5) Goldfarb, T. D. *Chemosphere* **1989**, *18*, 1051–1055.
(6) Dickson, L. C.; Karasek, F. W. *J. Chromatogr.* **1987**, *389*, 127–137.
(7) Eiceman, G.; Rghei, H. *Chemosphere* **1982**, *11*, 833–839.
(8) Rghei, H. O.; Eiceman, G. A. *Chemosphere* **1982**, *11*, 569–576.
(9) Rghei, H. O.; Eiceman, G. A. *Chemosphere* **1984**, *13*, 421–426.
(10) Rghei, H. O.; Eiceman, G. A. *Chemosphere* **1985**, *14*, 259–265.
(11) Vogg, H.; Metzger, M.; Stieglitz, L. *Waste Manage. Res.* **1987**, *5*, 285–294.
(12) Vogg, H.; Stieglitz, L. *Chemosphere* **1986**, *15*, 1373–1378.
(13) Stieglitz, L.; Vogg, H. *Chemosphere* **1987**, *16*, 1917–1922.
(14) Hagenmaier, H.; Kraft, M.; Brunner, H.; Haag, R. *Environ. Sci. Technol.* **1987**, *21*, 1080–1084.
(15) Lustenhouwer, J. W. A.; Olie, K.; Hutzinger, O. *Chemosphere* **1980**, *9*, 501–522.
(16) Stieglitz, L.; Zwick, G.; Beck, J.; Roth, W.; Vogg, H. *Chemosphere* **1989**, *18*, 1219–1226.
(17) Karasek, F. W.; Dickson, L. C. *Science* **1987**, *237*, 754–756.
(18) Dickson, L. C.; Lenoir, D.; Hutzinger, O. *Chemosphere* **1989**, *19*, 77–82.
(19) Dickson, L. C.; Lenoir, D.; Hutzinger, O. *Environ. Sci. Technol.* **1992**, *26*, 1822–1828.
(20) Deacon, H. W. British Patent 1403/1863; U.S. Patent 85370/1868; U.S. Patent 141.33.
(21) Griffin, R. D. *Chemosphere* **1986**, *15*, 1987–1990.
(22) Bruce, K. R.; Beach, L. O.; Gullett, B. K. *Waste Manage.* **1991**, *11*, 97–102.
(23) Yang, M.; Karra, S. B.; Senkan, S. M. *Hazard Waste Hazard. Mater.* **1987**, *4*, 55–68.
(24) Eiceman, G. A.; Rghei, H. O. *Environ. Sci. Technol.* **1982**, *16*, 53–56.
(25) Gullett, B. K.; Bruce, K. R.; Beach, L. O. *Waste Manage. Res.* **1990**, *8*, 203–214.
(26) Solomons, T. W. G. *Organic Chemistry*; John Wiley & Sons, Inc.: New York, 1976; p 452.
(27) de Leer, E.; Lexmon, R.; de Zeeuw, M. *Chemosphere* **1989**, *19*, 1141–1152.
(28) Sakai, S.; Hiraoka, M.; Takeda, M.; Nie, P.; Ito, T. Formation and degradation of PCDDs/PCDFs in a laboratory scale

Table 1 - CHARACTERISTICS OF MAJOR LIME AND LIMESTONE PRODUCTS AND BY-PRODUCTS

Reagent	Chemical Formula or Approximate Composition	Bulk Density (Kg/m^3)	Slurry pH
High calcium quicklime	CaO	769-1121	10.5-12.4
Dolomitic quicklime	$CaO \cdot MgO$	790-1400	9.0
High calcium hydrate	$Ca(OH)_2$	400-641	10.5-12.4
Normal dolomitic hydrate	$Ca(OH)_2 \cdot MgO$	400-560	9.0
Dolomitic pressure hydrate	$Ca(OH)_2 \cdot Mg(OH)_2$	480-640	9.0
High calcium limestone	$CaCO_3$	---	6.5
Dolomitic limestone	$CaCO_3 \cdot MgCO_3$	---	---*
Lime kiln dust	Generally 10-15% lime	---	varies up to 12.4
Cement kiln dust	Lime content varies	---	varies up to 12.4
Fly ash **	Lime content varies with type of coal	---	varies up to 12.4
Waste lime	Lime content varies with source	---	varies up to 12.4

* Non-reactive

** High calcium fly ash may have up to 2.4% uncombined CaO[3]

All waste that are hazardous can only be placed in specially designed landfills that include provisions for containing leachate from the waste and have cap materials that will minimize moisture movement through the waste. A stringent ground-water monitoring program is required on any hazardous waste landfill. Hazardous waste landfills act as buried storage for industrial wastes. Hazardous waste landfills are assumed to continue to be hazardous into the indefinite future.

Conventional wastes, those not requiring special handling, also must be placed in landfills that are designed to provide protection for the local ground water. Because of the lower risk, less stringent containment requirements apply and monitoring efforts are not as intense. Conventional waste landfills accept much of the biodegradable household waste, such as food, paper, and yard trash. The waste undergoes decomposition or stabilization during burial and the character of the waste draining through the landfill changes with age. Microbial decomposition of the buried refuse produces a mixture of carbon dioxide and methane gas and a variety of water soluble decomposition products; largely organic acids. Metals in the landfill are brought into solution in the acid leachate and metal levels in the leachate discharged from a conventional landfill can be much higher than in potable water. The waste itself changes during decomposition, generally becoming denser and more compact. The surface of the landfill will often subside (up to 3-4% during the first two or three years) as the refuse below it compacts. Structures built over a landfill can be damaged during subsidence. Foundations may crack and buried utility lines can be broken.

The two major types of landfills represent two widely different disposal philosophies and two different requirements for engineering design. The hazardous waste landfill is a perpetual burial site with total containment and no secondary use for the land above the site. The conventional landfill is an active decomposition system that will give off decomposition products in water or gases leaving the fill. After active decomposition ceases, secondary use of a conventional landfill is often possible. Lime, because it can be used to control the solubility of potential pollutants and can take part in cementitious reactions can be useful in both types of landfill design.

Landfill Designs - Both conventional and hazardous waste landfill designs contain three specific components (Figure 1):

1) A liner system developed to prevent contaminants from moving into the soil and ground water below the landfill.
2) The compacted waste material that supports the cover.
3) A capping system developed to prevent precipitation from moving into the landfilled waste.

These three basic components of the landfill can all be improved by careful consideration of performance requirements. For example, in many landfills it is not necessary to make a liner completely watertight if the liner material can be made to stop contaminant movement while allowing water to drain from the fill. Lime, because of its ability to control the chemical character of contacting water has been valuable in all three landfill components.

Lime in Landfill Liners - Alkaline liners containing layers of lime or limestone have been proposed and tested in both conventional and hazardous waste landfills. Initial results indicate that toxic metals are precipitated and acid wastes are neutralized in passing through a layer of lime or limestone below the waste.

Artiola and Fuller [4, 5] investigated the use of agricultural lime (calcium carbonate) as a chemical barrier below a conventional landfill. Acidic leachate percolated into the alkaline aggregate and potentially toxic metals were precipitated in the limestone filter layer. Limestone is a relatively ineffective reagent for acid neutralization [2]; the addition of hydrated lime improves performance. A hydrated lime soil liner has been tested for use in containment of toxic metals from uranium tailings piles [6]. The test liners were made by mixing 5% (by weight) of fine-grained (< 200 mesh) hydrated lime with a local sandy loam. Acidic, metal-rich water from uranium tailings ponds was passed through sandy loam with and without alkali-addition. The sandy loam alone had little effect on solution chemistry. After 17 pore volumes of water had passed through the untreated soil, the total dissolved solids (TDS) content of the effluent was higher than the influent liquid. The lime-ammended soil, in contrast, continued to reduce the TDS of the effluent even after 17 pore volumes had passed through the soil. The porosity and permeability of the lime-amended soil was greatly reduced by precipitation of contaminants in intergranular spaces in the soil. Initially the ammended soil had a permeability of 3.5×10^{-6} cm/sec; after 20 pore volumes of the acidic waste had passed the column the permeability decreased to 4×10^{-8} cm/sec. In

(15)

Philip G. Malone[1] and James H. May

THE USE OF LIME IN THE DESIGN OF LANDFILLS FOR WASTE DISPOSAL

REFERENCE: Malone, P. G. and May, J. H. "Use of Lime in the Design of Landfills for Waste Disposal," Symposium on Lime.

ABSTRACT: Lime and products containing lime have been widely employed in landfills. Examples of the use of lime in caps, wastes and liners are presented. Lime can provide a valuable chemical barrier to the transport of specific contaminants. Lime-pozzolan cements can be used to improve handling of wastes and decrease waste compaction. Lime-soil mixtures can be employed as impermeable, chemically-reactive liners.

Well documented demonstration projects are required to obtain data needed for the acceptance of lime-augmented landfill designs. Where waste containing lime are employed, standards should be presented as to the chemical characteristics of waste that make them acceptable.

[1] Geotechnical Laboratory, U. S. Army Engineers Waterways Experiment Station, Vicksburg, MS 39180-0631.

Introduction. - Lime (calcium hydroxide) and blended lime materials have long had a role in waste disposal because they can be inexpensively used to neutralize acidity and control the pH of waste materials [1-2]. Additionally lime can react with finely-divided, siliceous materials to produce cements that bond together particulate waste to improve handling or assist in isolating potentially toxic compounds by surrounding them with an inert calcium silicate complex. Unslaked lime or quicklime can be used to remove water from semisolid wastes and improve their handling characteristics.

The purpose of this report is to review and evaluate applications of lime in landfill designs as they are reported in the technical and engineering literature and to discuss how lime products and lime/waste blends can be most advantageously used in solid waste burial. Lime is a family of products that can be best employed when the engineering design of a disposal area takes advantage of the different properties of various lime products and lime blends to produce the physical and chemical conditions that favor waste containment.

Types of Lime - Many discussions on the use of lime in waste disposal treat all lime products as a single material or differentiate only between quicklime and hydrated lime, or discuss waste materials containing lime as if they were lime products. Many lime products and by-products behave differently and it is important to make distinctions in the type of material used. Table 1 lists the major products, by-products and wastes employed in waste treatment and summarizes their properties. Many of the by-products and waste products are poorly defined and the use of these materials in place of lime often requires the by-products be analysed on a batch-by-batch basis to assure that enough lime is available to produce the neutralization or cementation that is desired.

Types of Wastes. - Current regulations recognize two levels of land disposal operations; those for hazardous wastes and those for non-hazardous waste [3]. The hazardous wastes are defined as those wastes:

1) derived from an industrial process known to produce toxic or hazardous residues,
2) containing a substance that is classed as acutely toxic, or
3) deemed to be toxic on the basis of testing that demonstrates the waste exhibits some hazardous characteristic such as toxicity, reactivity or corrosivity.